RNA Structures

Monitoring Molecular Recognition of the Ribosomal Decoding Site**

*Sarah Shandrick, Qiang Zhao, Qing Han, Benjamin K. Ayida, Masayuki Takahashi, Geoffrey C. Winters, Klaus B. Simonsen, Dionisios Vourloumis, and Thomas Hermann**

Fidelity during protein synthesis is maintained by the ribosomal decoding site which monitors base pairing between the mRNA codon and the tRNA anticodon.[1] Binding of cognate tRNA induces conformational changes in ribosomal RNA (rRNA) at the decoding site that translate into a signal for the progression of translation. An internal loop containing adenine residues A1492 and A1493 in 16S rRNA of the 30S (small) ribosomal subunit constitutes a major component of the bacterial decoding site (Figure 1a). Contacts of the

[*] S. Shandrick, Dr. Q. Zhao, Dr. Q. Han, Dr. T. Hermann
Department of Structural Chemistry
Anadys Pharmaceuticals, Inc.
9050 Camino Santa Fe, San Diego, CA 92121 (USA)
Fax: (+1) 858-527-1539
E-mail: thermann@anadyspharma.com
Dr. B. K. Ayida, M. Takahashi, G. C. Winters, Dr. K. B. Simonsen, Dr. D. Vourloumis
Department of Medicinal Chemistry
Anadys Pharmaceuticals, Inc.

[**] S.S. and Q.Z. contributed equally. This work was supported in part by the National Institutes of Health (Grant AI51104 to T.H.). We are grateful to Prof. Yitzhak Tor, University of California, San Diego, for helpful discussions and suggestions that initiated our interest in using 2-aminopurine as a fluorescence label.

Supporting information for this article is available on the WWW under http://www.angewandte.org or from the author.

 DOI: 10.1002/ange.200454217

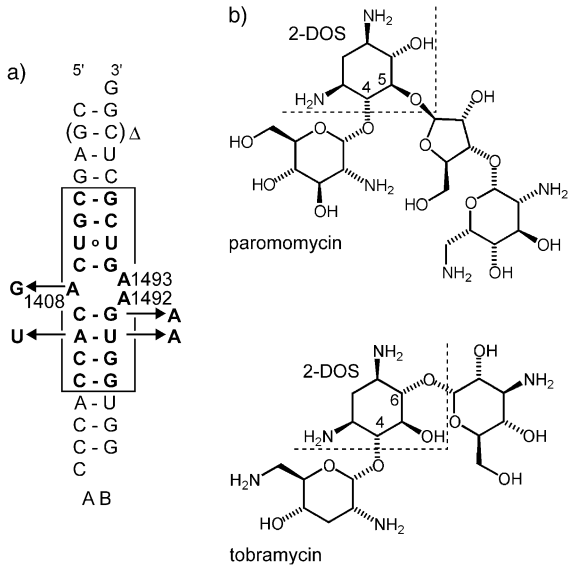

Figure 1. a) Bipartite oligonucleotide constructs AB and ABΔ containing the ribosomal decoding site used in this study. The box indicates the sequence that is identical to the bacterial decoding site. In the ABΔ RNA, one G–C base pair (in parentheses) is deleted in the upper flanking stem. Base changes in the eukaryotic sequence are indicated by arrows. The individual single-stranded oligonucleotides are referred to as A and B in the text. b) Aminoglycoside antibiotics paromomycin, a 4,5-disubstituted 2-deoxystreptamine, and tobramycin, a 4,6-disubstituted 2-deoxystreptamine (2-DOS = 2-deoxystreptamine).

conformationally flexible residues A1492 and A1493 across the shallow groove of the codon–anticodon hybrid have been proposed to be involved in sensing the base-pairing geometry between mRNA and tRNA, and discriminating against non-Watson–Crick alignments.[2] Aminoglycoside antibiotics increase the error rate of translation by binding specifically to the bacterial decoding-site RNA (Figure 1),[3] and locking the residues A1492 and A1493 in a conformation predisposed for interaction with the mRNA–tRNA hybrid. Pre-organization of part of the decoding site by bound aminoglycosides reduces the energetic cost of a ribosomal domain closure that is required for discrimination between noncognate and cognate tRNAs.[4] Insights into the molecular recognition of the decoding site by antibiotic ligands and the mechanics of translational fidelity are emerging from three-dimensional (3D) structures of aminoglycosides in complex with decoding-site oligonucleotides[5–7] and whole 30S ribosomal subunits.[8]

To explore specific aminoglycoside interactions with the bacterial decoding site as a model of RNA-targeting,[9] and as first step for the discovery of novel antibiotics, we have studied model oligonucleotides that retain the conformational flexibility of the decoding site in solution and that allow capture of distinct conformational states in RNA crystals. Fragments of rRNA containing the decoding site accurately represent the binding of natural aminoglycosides to the whole ribosome.[10–12] To facilitate direct comparison of solution binding experiments and crystallographic structure investigations, we focused on an RNA construct that could be used as a faithful model of the ribosomal decoding site, including its aminoglycoside binding properties, both in solution and crystallization studies. The bipartite oligonucleotides AB and ABΔ were chosen as optimal constructs, comprising the bacterial decoding-site sequence and flanking auxiliary base pairs that were added to enhance the crystallizability (Figure 1a). Both RNAs behaved identically in the fluorescence experiments described herein. In contrast to monopartite tethered decoding-site oligonucleotides used in binding studies by others,[7,12,13] the AB RNAs do not contain an artificial loop structure that may interfere with ligand binding or crystallization.[14]

We crystallized the AB oligonucleotide, and determined its 3D structure by X-ray diffraction (Table 1). While a range of crystallization conditions resulted in well-diffracting crystals of AB and ABΔ, hanging-drop vapor diffusion eventually allowed the growth of RNA crystals that captured two conformational states of A1492 within the decoding site (Figure 2). Electron density was found consistent with 50% partial occupancy of the A1492 base inside the RNA loop and 50% in a flipped-out conformation. In the inside conformation, the base of A1492 is fully stacked on G1491 and forms a *cis*-Watson–Crick pair[15] with residue A1408 of the opposite strand (Figure 2b). The bases of A1492 and A1493 are partially stacked in the flipped-out conformation, which closely resembles the RNA structures in complexes of aminoglycosides bound to the decoding site.[5,6,8] We were able to soak the aminoglycoside paromomycin into crystals of AB containing the flipped-out conformation of A1492 and observe electron density consistent with the aminoglycoside bound at the decoding-site loop.[26]

The absence of crystal-packing contacts with A1492 in the flipped-out conformation in conjunction with the random distribution between the in- and out-states suggests that the two conformations are energetically similar. By variation of

Table 1: Crystal data and refinement statistics.

	AB native[a]	ABΔ-2AP1492[a]
resolution range [Å]	8.0–1.7	8.0–2.2
highest resolution shell [Å]	1.76–1.70	2.28–2.20
space group	$P2_12_12_1$	$P2_1$
unit cell: a, b, c [Å]	32.04, 32.95, 92.69	31.64, 87.32, 32.79
unit cell: β [°]	90	93.27
unique reflections (fold redundancy)	11,015 (14.9)	8,903 (8.6)
completeness [%]	97.0 (81.6)	99.1 (96.1)
$I/\sigma I$	32.7 (6.1)	15.3 (3.3)
R_{merge}[b]	0.044 (0.164)	0.09 (0.311)
R factor[c]	0.209 (0.337)	0.205 (0.299)
R_{free}[d]	0.238 (0.447)	0.266 (0.328)
RNA atoms	809	1396
solvent molecules	130	215
r.m.s.d. from ideality: bonds [Å]	0.023	0.004
r.m.s.d. from ideality: angles [°]	1.90	0.93
average B-factors [Å^2]: RNA	24.9	23.9
average B-factors [Å^2]: solvent	35.8	31.8

[a] Numbers in parentheses are statistics for data of the highest resolution shell, except for fold redundancy. [b] $R_{merge} = \Sigma_{hkl}\Sigma|I_i - \langle I\rangle|/\Sigma_{hkl}\Sigma I_i$ for all data with $I/\sigma I > -3$. [c] R factor $= \Sigma_{hkl}||F_{obs}| - k|F_{calcd}||/\Sigma_{hkl}|F_{obs}|$. [d] R_{free} was calculated from 10% of the data.

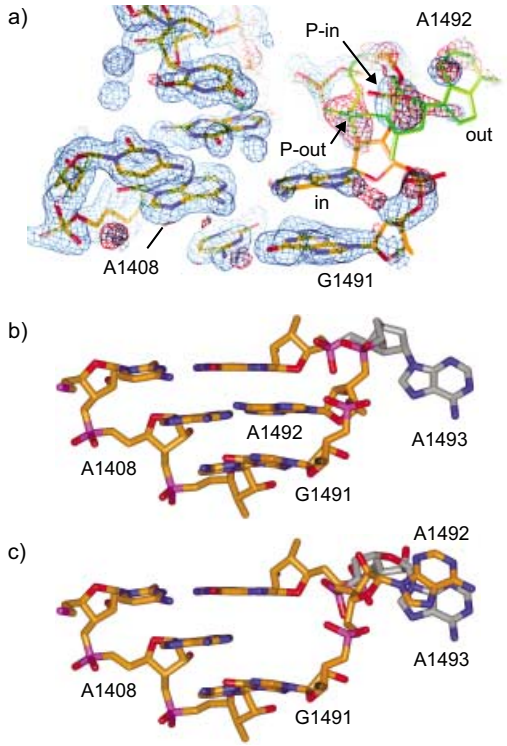

Figure 2. 3D structure of the decoding site in AB RNA as determined by X-ray diffraction of a crystal that captured a 1:1 random distribution of A1492 oriented inside and outside the RNA loop. a) Electron-density maps (blue: $2F_o-F_c$ contoured at 1.3σ; red: F_o-F_c at 3σ) around the decoding site, calculated using an AB model in which A1492 was oriented inside the RNA loop. For comparison, the flipped-out conformation of the A1492 residue is shown in green sticks (not included in map calculation). Positions of the phosphate groups (P) for the two conformations (in/out) are indicated (for density maps around a model with A1492 flipped out, see Supporting Information S1). b) Inside conformation of A1492 with the base stacking on G1491 in the interior of the decoding-site loop and forming a *cis*-Watson–Crick pair with residue A1408 of the opposite strand. c) Flipped-out conformation of A1492 with the base stacking partially on A1493 (gray sticks).

the conditions for crystallization of the AB and ABΔ RNAs, occupancy of either state could be driven to completeness. In contrast to the position of A1492, and independent from the crystallization conditions, the conformation of A1493 is locked in a flipped-out state by contacts in the shallow groove of a neighboring RNA helix (see Supporting Information).

To investigate the conformational states of the flexible residues A1492 and A1493 in solution, we replaced in ABΔ the adenines at either of these positions by the fluorescent 2-aminopurine (2-AP) base. This adenine analogue is a sensitive probe of structural environment since fluorescence of 2-AP is quenched when it is stacked with other bases, but increases significantly upon unstacking and exposure to solvent.[16,17] Alternative conformations of residues in the decoding site in the crystal structures of the AB RNAs are thus expected to give rise to distinct fluorescence intensities corresponding to the stacking state of the 2AP label. Indeed, the observed fluorescence signal of the ABΔ RNA constructs, 2AP-labeled at either position 1492 or 1493, agreed well with the distinct conformations of residues A1492 and A1493 in the crystal structures of AB and ABΔ (Figure 3a). The ABΔ RNA carrying 2AP at the 1492 position showed low fluorescence intensity, indicating that residue 2AP is stacked inside the

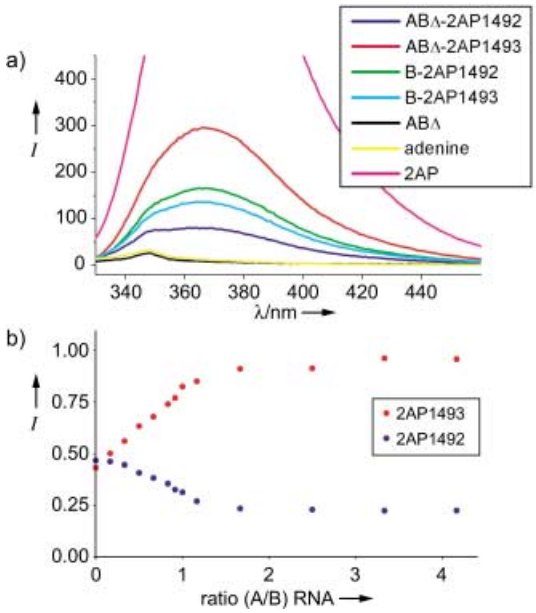

Figure 3. a) Fluorescence emission spectra of 2AP-labeled RNAs and controls at equivalent concentrations. ABΔ-2AP1492 = ABΔ RNA with 2AP at position 1492, ABΔ-2AP1493 = ABΔ RNA with 2AP at position 1493, B-2AP1492 = B oligonucleotide with 2AP1492, B-2AP1493 = B oligonucleotide with 2AP1493; Controls: ABΔ = unlabeled RNA construct; adenine and 2AP = monomeric bases. b) Normalized fluorescence signal at 370 nm during titration of single-stranded oligonucleotide A to single-stranded B that has the 2AP label at residue 1492 and 1493, respectively. (Experimentally determined oligonucleotide concentrations resulted in slight underestimation of the A/B ratio, presumably owing to the use of empirical extinction coefficients in RNA-concentration calculations.)

decoding-site loop. In contrast, the 2AP1493-labeled construct gave rise to high fluorescence, in line with a substantial solvent exposure of the 1493 residue. Fluorescence of the 2AP-labeled single-stranded B oligonucleotides (that is, in the absence of the A strand) was of an intermediate intensity, nearly independent from the position of the fluorescent base and perhaps reflecting little-defined conformations of the single-stranded RNA. The differences in fluorescence between the 2AP-labeled single-stranded B and double-stranded ABΔ RNAs were exploited to monitor structure formation in the decoding-site loop upon hybridization of the A and B oligonucleotides (Figure 3b). Titration of strand A to a constant amount of 2AP1493-labeled B resulted in a steady increase of fluorescence up to 1:1 stoichiometry of the oligonucleotides, after which the signal leveled off. The equimolar oligonucleotide ratio was marked by a clear inflection of the fluorescence signal, indicating that all the B strand was hybridized into ABΔ in which the flipped-out conformation of 2AP1493 resulted in high fluorescence. The precisely converse effect was observed when strand A was titrated to 2AP192-labeled B oligonucleotide. These data

further suggest that the flipped-out conformation of residue A1493 in the crystal structure of the decoding-site construct AB is not an artifact of crystal packing, but rather reflects the capture of a conformational state that is preferred in solution.

To examine if replacement of the adenine base at position 1492 disturbs the conformational states of the decoding-site loop, we determined the 3D structure of 2AP-labeled ABΔ RNA by X-ray crystallography. We were especially interested in the ABΔ-2AP1492 construct, as we assumed that the inside conformation of residue 1492 might be affected by the exchange of adenine to 2AP, while the preferentially flipped-out residue 1493 would be less sensitive to base identity. The structure of ABΔ-2AP1492 in crystals grown under similar conditions as described above for AB, had the 2AP1492 residue in alternating inside and flipped-out conformations, arranged in a symmetry-related fashion (Figure 4 and Table 1). The residue A1493 is pointing outside

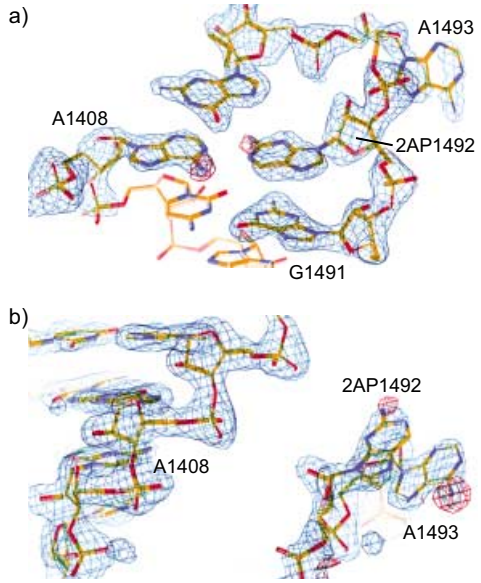

Figure 4. 3D structure of the decoding site in fluorescence-labeled ABΔ-2AP1492 RNA as determined by X-ray diffraction of a crystal that captured a symmetry-related 1:1 distribution of A1492 oriented inside and outside the RNA loop. a) Electron-density maps (blue: $2F_o-F_c$ contoured at 1.3σ; red: F_o-F_c at 2.8σ) around the decoding-site loop with 2AP1492 oriented inside the RNA. The exocyclic 2-amino group of 2AP1492 and 6-amino group of A1493 are omitted from the model used for density calculation, giving rise to F_o-F_c density that unambiguously revealed the identity of the adenine and 2AP bases. b) Electron density maps around the decoding-site loop with 2AP1492 in the flipped-out state.

in all ABΔ-2AP1492 RNA molecules and involved in similar packing contacts as those observed in the AB RNA structure. In the inside-conformation of 2AP1492, the fluorescent base stacks on G1491, whereas in the flipped-out state, it is stacked on A1493 (see Supporting Information).

The conformation of the decoding-site loop in both states of the ABΔ-2AP1492 RNA closely resembles the structure of the unlabeled AB RNA, with exception of the 2AP1492–A1408 base pair in the inside conformation. Compared to the canonical *cis*-Watson–Crick geometry of the A1492–A1408 pair in the crystal structure of AB, the 2AP1492 residue in ABΔ-2AP1492 is rotated slightly towards the shallow groove to accommodate the 2-amino group. The 2AP1492–A1408 pair is stabilized by two hydrogen bonds, (A1408)N6-H···N1(2AP1492) and (2AP1492)N2-H···N1(A1408). The similarity of the native and 2AP-labeled constructs, both with regard to 3D structure as well as the geometry and conformational states of residues 1492 and 1493, led us to conclude that the modified RNAs might be used as sufficiently faithful representatives of the decoding-site in fluorescence measurements of aminoglycoside binding.

We reasoned that the fluorescence intensity changes associated with conformational rearrangements of residue 1492 in the 2AP-labeled decoding-site RNA might be exploited to monitor the interaction of ligands with the internal loop (Figure 5a). The aminoglycoside paromomycin was used as a representative ligand (Figure 1b), since structural investigations had shown earlier that upon binding this natural product induces the residues A1492 and A1493 to flip out of the decoding-site loop.[5,6,8] We performed titrations of paromomycin to a variety of 2AP-labeled decoding-site constructs (Figure 5b and Supporting Information). As a control, paromomycin was also added to 2AP monomer, 2AP-labeled single-strand B oligonucleotide (not shown), and double-labeled (1492 and 1493) ABΔ RNA, none of which showed significant changes of fluorescence. In contrast, titration of the aminoglycoside to 2AP1492-labeled ABΔ RNA lead to a dramatic increase of fluorescence, corresponding to an EC_{50} value (EC_{50} is the concentration required for 50% response) of 0.75 ± 0.05 μM for the paromomycin dose response. Fluorescence of 2AP1493-labeled ABΔ construct was quenched by paromomycin at an EC_{50} value that was identical within the experimental error (0.95 ± 0.20 μM). The EC_{50} values calculated from both experiments are in good agreement with the binding affinity of paromomycin for decoding-site RNA ($K_d \approx 10^{-6}$ M).[11,12] The congruence of the fluorescence changes triggered by paromomycin addition to either the 2AP1492- or 2AP1493-labeled construct indicates that the same conformational event is monitored in both cases, and that the 2AP label does not alter the interaction of the aminoglycoside with the RNA target. We suggest that binding of paromomycin to the decoding site displaces residue 1492 from the internal loop, associated with unstacking of the base and increase of 2AP1492 fluorescence. As demonstrated by the structural studies on the decoding site, the flipping-out of A1492 forces the bases of residues 1492 and 1493 to partially stack onto each other, which leads to quenching of the 2AP1493 fluorescence. That fluorescence of 2AP1492-labeled RNA increases above the level of 2AP1493-labeled construct in the paromomycin-bound state (Figure 5b), although residues 1492 and 1493 are mutually stacked, might be attributed to the asymmetric overlap of the bases (see Supporting Information) and their distinct solvation, both of which influence the quantum yield of the fluorophore.[17]

The preferentially flipped-out conformation of residue 1493 renders this position ideally suited for fluorescence labeling since base modifications are unlikely to interfere with either the structural integrity of the decoding site or with

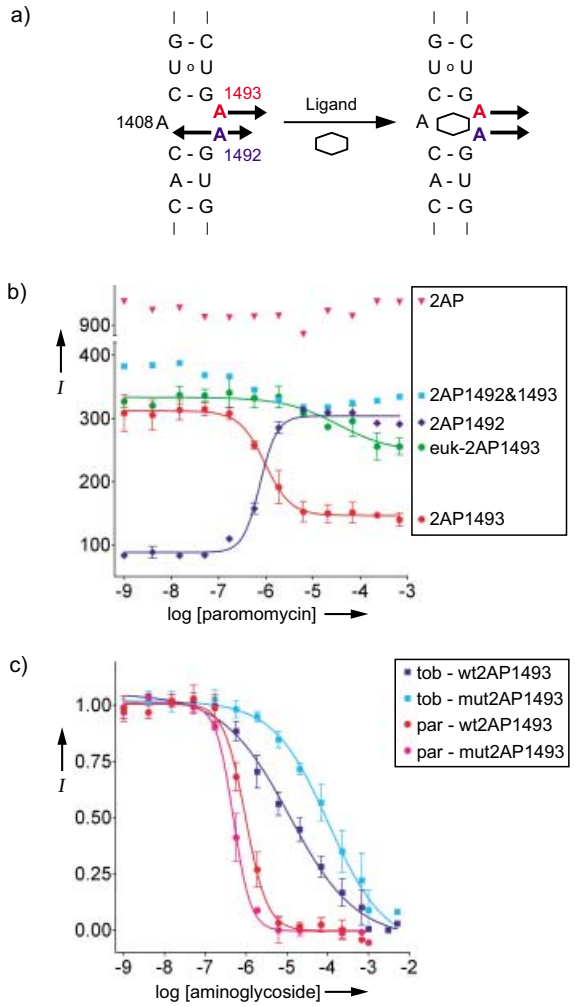

Figure 5. a) Model illustrating the conformational changes triggered by aminoglycoside ligand binding to the AB decoding-site RNA. See text for a discussion. b) Titrations of 2AP-labeled RNA constructs and 2AP monomer with paromomycin (see text for details). The fluorescence signal at 370 nm is plotted against log of aminoglycoside concentration (error bars correspond to 2σ calculated for the average of two experiments). c) Titrations of 2AP-labeled wild-type decoding site (wt2AP1493) and U1406A mutant construct (mut2AP1493) with paromomycin (par) and tobramycin (tob). Normalized fluorescence signals are plotted.

ligand binding. The concept of indirect fluorescence quenching by ligand-induced displacement of A1492 and stacking on residue 1493 can therefore be extended to other labels which have fluorescent characteristics that make them suitable for the testing of UV-active decoding-site ligands. Fluorescent pteridine base analogues, which have higher quantum yields along with emission maxima shifted to longer wavelengths,[18] may replace 2AP as the preferred label to prepare decoding-site constructs for ligand binding studies.[27]

The fluorescence-labeled RNA constructs described herein provide powerful probes to detect the specific binding of ligands to the ribosomal decoding-site and to discriminate against nonspecific RNA binders (see also Supporting Information). Importantly, 2AP-labeled RNA models of the eukaryotic decoding site can be used to investigate the target selectivity of ligand binding. Titration of paromomycin to a 2AP-labeled RNA construct that carried the eukaryotic decoding-site sequence (Figure 1a) exhibited significantly lower affinity of the aminoglycoside for the eukaryotic compared to the bacterial target (euk-2AP1493, Figure 5b), substantiating the organism-specificity of these antibiotics that is exploited in therapy.[12] Moreover, 2AP-labeled bacterial decoding-site constructs are useful tools with which to investigate the molecular discrimination associated with target mutations in aminoglycoside-resistant bacteria. As an example, we have tested aminoglycoside interaction with bacterial decoding-site RNA that carried the U1406A mutation, which is known to confer resistance selectively to 4,6-disubstituted 2-DOS (Figure 1b).[19] The binding of paromomycin, a 4,5-disubstituted 2-DOS, is little affected by the mutation, whereas the affinity of tobramycin, which belongs to the 4,6-disubstituted 2-DOS class (Figure 1b), is noticeably reduced (Figure 5c). The EC_{50} values calculated for tobramycin binding to the wild type and U1406A mutant RNA (wt: 9.5 ± 2.0 μM; mut: 110 ± 8.5 μM) are in agreement with the minimum inhibitory concentration (MIC) shift for tobramycin in corresponding wild type and mutant bacteria reported by Pfister and co-workers.[20] Crystal-structure analyses by Vicens and Westhof have shown that the U1406A substitution causes steric clash between the exocyclic amino group of A1406 and the sugar ring linked at the 6-position of 2-DOS.[6] Molecular discrimination resulting from the U1406A target mutation is well reproduced by the 2AP-labeled decoding-site RNAs.

In summary, we have developed a set of fluorescence-labeled RNA constructs to investigate molecular recognition of the ribosomal decoding site, the target of many aminoglycoside antibiotics. Incorporation of fluorescent 2AP has been used before to probe conformational changes of RNA in solution,[16,21] and while this manuscript was in preparation, Pilch and co-workers reported a similar concept for detecting conformational changes in ribosomal RNA by 2AP replacement of A1492.[13] In the study described herein, we have combined structural data from X-ray crystallography and fluorescence measurements in a unique fashion to explore the conformational states of the decoding site. We exploited the indirect quenching of fluorescence-labeled residue 1493 by a conformational change in A1492, which is in turn induced by specific ligand binding to the decoding site. The approach disclosed herein provides a basis for affinity screening of the ribosomal target against novel RNA binders as highly selective lead candidates for the discovery of novel antibiotics. Consequently, our group has extensively used the fluorescence binding assay for the decoding-site target to establish structure–affinity relationships for designed aminoglycoside mimetics.[22]

Experimental Section

Gel-purified and desalted oligonucleotides (Figure 1, constructs AB and ABΔ) were purchased from Dharmacon Research (Lafayette, CO). Double-stranded RNA was obtained by heating complementary oligonucleotides in buffer at 75 °C for 1 min and snap cooling on ice. Cacodylate buffer (30 mM, pH 6.8) was used to prepare RNA for

crystallization, and cacodylate or phosphate buffer (30 mM, pH 6.8) for fluorescence experiments.

Fluorescence measurements were performed on an RF-5301PC spectrofluorometer (Shimadzu, Columbia, MD) at 25 °C. Emission spectra were recorded at 1 μM RNA concentration in 1-cm path-length quartz cells, irradiating at 310 nm. EC_{50} values were calculated with the ORIGIN software (MicroCal, Northampton, MA) by fitting a dose response curve to the fluorescence intensity plotted against the log of ligand concentration.

RNA was crystallized by the hanging-drop vapor-diffusing method using sparse matrix screens (Hampton Research, Aliso Viejo, CA). Crystals of decoding-site constructs (0.3 mM RNA) grew within 2 weeks from 1.95 to 2.05 M ammonium sulfate, 50 mM Na cacodylate (pH 6.8), and 0.7 to 1.2 mM Mg acetate. For X-ray diffraction, crystals were transferred to glycerol (15% v/v) as a cryoprotectant and frozen. Data sets were collected with an R-AXIS IV imaging plate detector using $Cu_{K\alpha}$ radiation ($\lambda = 1.54178$ Å) of an RU-H3R rotating anode generator (Rigaku/MSC, The Woodlands, TX). Data were processed with DENZO/SCALEPACK.[23] Structures were solved by molecular replacement using canonical A-form RNAs as the initial model with AMORE,[24] and refined with CNS.[25] For crystal data and refinement statistics see Table 1. Coordinates and structure factors have been deposited in the Protein Data Bank (accession codes 1T0E and 1T0D for native decoding site and 2-AP labeled RNA, respectively).

Received: March 9, 2004 [Z54217]

Keywords: antibiotics · fluorescent probes · molecular recognition · RNA structures · structure elucidation

[1] J. M. Ogle, A. P. Carter, V. Ramakrishnan, *Trends Biochem. Sci.* **2003**, *28*, 259 – 266.
[2] J. M. Ogle, D. E. Brodersen, W. M. Clemons, M. J. Tarry, A. P. Carter, V. Ramakrishnan, *Science* **2001**, *292*, 897 – 902.
[3] D. Moazed, H. F. Noller, *Nature* **1987**, *327*, 389 – 394.
[4] J. M. Ogle, F. V. Murphy, M. J. Tarry, A. P. Carter, V. Ramakrishnan, *Cell* **2002**, *111*, 721 – 732.
[5] a) Q. Vicens, E. Westhof, *Structure* **2001**, *9*, 647 – 658; b) Q. Vicens, E. Westhof, *J. Mol. Biol.* **2003**, *326*, 1175 – 1188.
[6] Q. Vicens, E. Westhof, *Chem. Biol.* **2002**, *9*, 747 – 755.
[7] D. Fourmy, M. I. Recht, S. C. Blanchard, J. D. Puglisi, *Science* **1996**, *274*, 1367 – 1371.
[8] A. P. Carter, W. M. Clemons, D. E. Brodersen, R. J. Morgan-Warren, B. T. Wimberly, V. Ramakrishnan, *Nature* **2000**, *407*, 306 – 307.
[9] a) T. Hermann, *Angew. Chem.* **2000**, *112*, 1962 – 1979; *Angew. Chem. Int. Ed.* **2000**, *39*, 1890 – 1904; b) Y. Tor, *ChemBioChem* **2003**, *4*, 998 – 1007; c) Q. Vicens, E. Westhof, *ChemBioChem* **2003**, *4*, 1018 – 1023.
[10] a) P. Purohit, S. Stern, *Nature* **1994**, *370*, 659 – 662; b) H. Miyaguchi, H. Narita, K. Sakamoto, S. Yokoyama, *Nucleic Acids Res.* **1996**, *24*, 3700 – 3706.
[11] M. I. Recht, D. Fourmy, S. C. Blanchard, K. D. Dahlquist, J. D. Puglisi, *J. Mol. Biol.* **1996**, *262*, 421 – 436.
[12] a) C. H. Wong, M. Hendrix, E. S. Priestley, W. A. Greenberg, *Chem. Biol.* **1998**, *5*, 397 – 406; b) R. H. Griffey, S. A. Hofstadler, K. A. Sannes-Lowery, D. J. Ecker, S. T. Crooke, *Proc. Natl. Acad. Sci. USA* **1999**, *96*, 10129 – 10133; c) S. R. Lynch, J. D. Puglisi, *J. Mol. Biol.* **2001**, *306*, 1037 – 1058.
[13] M. Kaul, C. M. Barbieri, D. S. Pilch, *J. Am. Chem. Soc.* **2004**, *126*, 3447 – 3453.
[14] E. Ennifar, A. Nikulin, S. Tishchenko, A. Serganov, N. Nevskaya, M. Garber, B. Ehresmann, C. Ehresmann, S. Nikonov, P. Dumas, *J. Mol. Biol.* **2000**, *304*, 35 – 42.
[15] N. B. Leontis, J. Stombaugh, E. Westhof, *Nucleic Acids Res.* **2002**, *30*, 3497 – 3531.
[16] a) D. C. Ward, E. Reich, L. J. Stryer, *J. Biol. Chem.* **1969**, *244*, 1228 – 1237; b) D. P. Millar, *Curr. Opin. Struct. Biol.* **1996**, *6*, 322 – 326.
[17] a) A. Bierzynski, H. Kozlowska, K. I. Wierzchowski, *Biophys. Chem.* **1977**, *6*, 223 – 229; b) J. M. Jean, K. B. Hall, *Proc. Natl. Acad. Sci. USA* **2001**, *98*, 37 – 41; c) E. L. Rachofsky, R. Osman, J. B. Ross, *Biochemistry* **2001**, *40*, 946 – 956; d) J. M. Jean, K. B. Hall, *Biochemistry*, **2002**, *41*, 13152 – 13161.
[18] M. E. Hawkins, *Cell Biochem. Biophys.* **2001**, *34*, 257 – 281.
[19] a) H. Taniguchi, B. Chang, C. Abe, Y. Nikaido, Y. Mizuguchi, S. I. Yoshida, *J. Bacteriol.* **1997**, *179*, 4795 – 4801; b) M. I. Recht, J. D. Puglisi, *Antimicrob. Agents Chemother.* **2001**, *45*, 2414 – 2419.
[20] P. Pfister, S. Hobbie, Q. Vicens, E. C. Böttger, E. Westhof, *ChemBioChem* **2003**, *4*, 1078 – 1088.
[21] a) M. Menger, T. Tuschl, F. Eckstein, D. Pörschke, *Biochemistry* **1996**, *35*, 14710 – 14716; b) I. Zagorowska, R. W. Adamiak, *Biochimie* **1996**, *78*, 123 – 130; c) S. R. Kirk, N. W. Luedtke, Y. Tor, *Bioorg. Med. Chem.* **2001**, *9*, 2295 – 2301; d) N. G. Walter, D. A. Harris, M. J. Pereira, D. Rueda, *Biopolymers* **2001**, *61*, 224 – 242.
[22] a) K. B. Simonsen, B. K. Ayida, D. Vourloumis, M. Takahashi, G. C. Winters, S. Barluenga, S. Qamar, S. Shandrick, Q. Zhao, T. Hermann, *ChemBioChem* **2002**, *3*, 1223 – 1228; b) D. Vourloumis, G. C. Winters, M. Takahashi, K. B. Simonsen, B. K. Ayida, S. Shandrick, Q. Zhao, T. Hermann, *ChemBioChem* **2003**, *4*, 879 – 885; c) K. B. Simonsen, B. K. Ayida, D. Vourloumis, G. C. Winters, M. Takahashi, S. Shandrick, Q. Zhao, T. Hermann, *ChemBioChem* **2003**, *4*, 886 – 890; d) S. Barluenga, K. B. Simonsen, E. S. Littlefield, B. K. Ayida, D. Vourloumis, G. C. Winters, M. Takahashi, S. Shandrick, Q. Zhao, Q. Han, T. Hermann, *Bioorg. Med. Chem. Lett.* **2004**, *14*, 713 – 718.
[23] Z. Otwinowski, W. Minor, *Methods Enzymol.* **1997**, *276*, 307 – 326.
[24] J. Navaza, *Acta Crystallogr. Sect. A* **1994**, *50*, 157 – 163.
[25] A. T. Brünger, P. D. Adams, G. M. Clore, W. L. DeLano, P. Gros, R. W. Grosse-Kunstleve, J.-S. Jiang, J. Kuszewski, M. Niges, N. S. Pannu, R. J. Read, L. M. Rice, T. Simonson, K. L. Warren, *Acta Crystallogr. Sect. D* **1998**, *54*, 905 – 921.
[26] Q. Han, T. Hermann, unpublished results.
[27] S. Shandrick, T. Hermann, unpublished results.

